



Article

Macro- and Micromechanical Assessment of the Influence of Non-Plastic Fines and Stress Anisotropy on the Dynamic Shear Modulus of Binary Mixtures

Meisam Goudarzy * and Debdeep Sarkar

Chair of Soil Mechanics, Foundation Engineering and Environmental Geotechnics, Ruhr-Universität Bochum, 44801 Bochum, Germany; debdeep.sarkar@rub.de

* Correspondence: meisam.goudarzychore@rub.de; Tel.: +4-923-4322-6078

Abstract: Resonant column tests were carried out on Hostun sand mixed with 5%, 10% and 20% non-plastic fines (defined as grains smaller than 0.075 mm) in order to quantify the combined influence of the void ratio (e), anisotropic stress state (defined as σ_v'/σ_h') and fines content (f_c) on the maximum small-strain shear modulus G_{max} . A significant reduction in the G_{max} with increasing f_c was observed. Using the empirical model forwarded by Roesler, the influence of e and σ_v'/σ_h' on G_{max} was captured, although the model was unable to capture the influence of varying fines content using a single equation. From the micro-CT images, a qualitative observation of the initial skeletal structure of the 'fines-in-sand' grains was performed and the equivalent granular void ratio e^* was determined. The e was henceforth replaced by e^* in Roesler's equation in order to capture the variation in f_c . The new modification was quantified in terms of the mean square error R^2 . Furthermore, the G_{max} of Hostun sand–fine mixtures was predicted with good accuracy by replacing e with e^* . Additionally, a micromechanical interpretation based on the experimental observation was developed.



Citation: Goudarzy, M.; Sarkar, D. Macro- and Micromechanical Assessment of the Influence of Non-Plastic Fines and Stress Anisotropy on the Dynamic Shear Modulus of Binary Mixtures. *Fractal Fract.* **2022**, *6*, 205. <https://doi.org/10.3390/fractalfract6040205>

Academic Editor: Wojciech Sumelka

Received: 28 February 2022

Accepted: 4 April 2022

Published: 6 April 2022

Publisher's Note: MDPI stays neutral with regard to jurisdictional claims in published maps and institutional affiliations.



Copyright: © 2022 by the authors. Licensee MDPI, Basel, Switzerland. This article is an open access article distributed under the terms and conditions of the Creative Commons Attribution (CC BY) license (<https://creativecommons.org/licenses/by/4.0/>).

Keywords: anisotropic stress; Hostun sand; resonant column; maximum shear modulus; fines content; void ratio; equivalent granular void ratio

1. Introduction

The determination of soil stiffness is of primary importance, considering its application in practical fields of geotechnical engineering, including foundation settlements, deformations caused by excavations or wave propagation in the ground due to vibration. In addition, all geotechnical sub/superstructure designs require the soil stiffness parameters in order to estimate the resistance of a structure against dynamic motions, such as earthquakes. In recent years, the development of elasto-plastic and advanced constitutive models (e.g., hardening soil model with small-strain stiffness, SANISAND) exclusively requires the small-strain soil stiffness parameter G_{max} as an input, underlining its importance in terms of research and practice in the field of soil dynamics.

Soil stiffness typically has a maximum value at low strains (strain $< 10^{-6}$), denoted either G_{max} or G_0 , and decreases by increasing the strain amplitude. Since the 1960s, several researchers ([1–3]) identified the influence of the void ratio and the effective stress on the small-strain shear modulus G_{max} . The authors of [1] were the earliest to formulate an empirical equation to capture the influence of the void ratio and effective stress under isotropic stress conditions (Equation (1)):

$$G_{max} = A p_a f(e) \left(\frac{p'}{p_a} \right)^n \quad (1)$$

where A is a material constant depending on the soil type, p_a is the atmospheric pressure (≈ 100 kPa), p' is the effective stress, n is a stress exponent and $f(e)$ is the void ratio function, which popularly takes the form of Equation (2) ([1]) or Equation (3) ([4]):

$$f(e) = \frac{(c - e)^2}{1 + e} \quad (2)$$

$$f(e) = e^{-d} \quad (3)$$

c and d are fitting parameters. The authors of [5,6] studied the influence of the grain size distribution on G_{max} , where they reported a significant influence of the uniformity coefficient C_u and the mean grain size D_{50} , which they characterized via empirical relations. Other than grain size, the fines content (i.e., grains passing through a standard US 200 sieve and smaller than 0.075 mm) can also influence the mechanical behavior of soils, as was evidenced in previous studies, e.g., refs. [7–11]. Systematic studies on the effect of fines content and isotropic stress on G_{max} have been published by [8–18]. These studies showed a strong influence of the non-cohesive fines fraction on G_{max} —a decrease in G_{max} was observed with increasing fines content. Therefore, ref. [12] proposed a reduction factor for Equation (1), as shown in Figure 1.

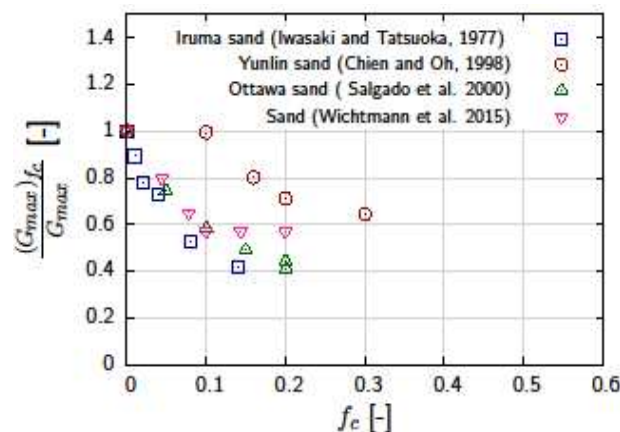


Figure 1. Reduction factor accompanying Equation (1) recommended by [12] to capture the influence of non-plastic fines on the maximum small-strain shear stiffness G_{max} .

It must be noted that Equation (1), in conjunction with the reduction factor, is not very suitable since it assumes different values for each soil type, as demonstrated by [17–19]. The authors of [9,11] reported that the fitting parameters of Equations (1)–(3) are influenced by fines content, which means for every binary mixture, the fitting parameters must be separately determined.

It is possible to capture the influence of the fines content on the mechanical behavior of granular soils by utilizing the concept of equivalent granular void ratio, as defined by [7]. Furthermore, ref [19] defined that a certain portion of fines actively participate in the granular structure contributing to force chains, based on which Equation (4) was suggested, where a boundary was formulated, below which the soil behavior would be dominated by sand (defined as ‘fines-in-sand’) and above which by fines (‘sand-in-fines’) ([19,20]).

$$e^* = \frac{e + (1 - b)f_c}{1 - (1 - b)f_c} \quad f_c < f_{thr} \quad (4)$$

The b -value holds a value between 0 and 1 and is responsible for denoting the active proportion of fines in the soil structure; therefore, it is a function of the fine content—the higher the value the higher the percentage of fines contributing to force chains in

the mixture. In [20,21], the authors developed a semi-empirical equation (Equation 5) to calculate b -parameter.

$$b = \left[1 - \exp \left\{ -0.3 \frac{(f_c / f_{thr})}{k} \right\} \right] \times \left(r \frac{f_c}{f_{thr}} \right)^r \tag{5}$$

where $r = (D_{10}/d_{50})^{-1}$, D_{10} = sand grain size corresponding to 10% finer materials by weight passing through, d_{50} = fine grain size corresponding to 50% finer materials by weight passing through, $k = (1 - r^{0.25})$. The authors of [17,19] had previously used this formulation in their work on binary mixtures.

Ref. [10] carried out resonant column (RC) tests on Hostun sand mixed with a fine fraction. They reported the significant influence of the fines content on the maximum shear modulus (Figure 2a). The concept of equivalent granular void ratio e^* [22,23] was successfully used to predict the maximum shear modulus in Equation (1) under isotropic stress conditions. However, no investigation was done for anisotropic stress states.

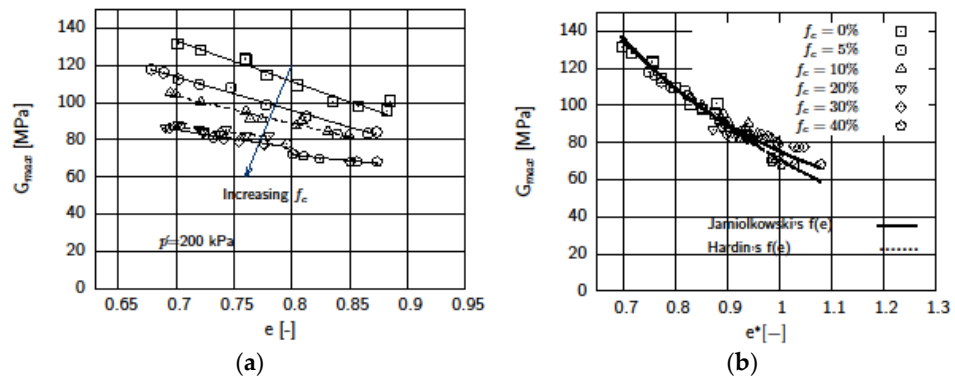


Figure 2. (a) Influence of fines content on the G_{max} via RC tests; (b) using the concept of equivalent granular void ratio e^* to capture varying percentages of fines content ([10]).

In order to evaluate the effect of anisotropy, numerous laboratory tests using bender elements ([11,24–30]), RC and torsional shear tests ([1,11,31–35]) have already been carried out. Furthermore, [1] and [24] extended the empirical relations to account for anisotropy. [1] believed that shear stress plays an insignificant role on shear modulus and suggested replacing p' in Equation (1) with the average of vertical and horizontal stresses Equation (6).

$$G_{max} = Af(e)p_a^{(1-n)} \left(\frac{\sigma_v + \sigma_h}{2} \right)^n \tag{6}$$

σ_v and σ_h denotes the vertical and horizontal stresses.

Ref. [24] conducted experimental studies on cubic soil samples to investigate the effects of stress components on shear wave velocity under anisotropic loading, where a significant influence of vertical stress on shear wave velocity and, consequently, on G_{max} was reported. Therefore, Hardin’s relationship was modified accordingly by using σ'_v and σ'_h instead of p' , as shown in Equation (7):

$$G_{max} = Af(e)p_a \left(\frac{\sigma'_v}{p_a} \right)^{n_v} \left(\frac{\sigma'_h}{p_a} \right)^{n_h} \left(\frac{\sigma_c}{p_a} \right)^{n_c} \tag{7}$$

n_v , n_h and n_c are the stress exponents, while σ_c represents the out-of-plane stress.

Furthermore, it was also found out that the placing technique of the sand does not influence the shear wave velocities. Reference [11] performed tests on glass beads, concluding that reference shear strain was affected by anisotropy, and an empirical relationship was developed, considering confining pressure and anisotropic stress components. Performing tests on Ticino sand under both horizontal and vertical directions using geophones

equipped with bender and compression elements, ref. [25] noted stiffnesses in the horizontal plane were larger than in the vertical plane. Using a similar procedure, ref. [26] investigated the interdependence of the active earth pressure coefficient K_0 on stress-induced anisotropy. The work of [24] was further extended by [27], in which the author attempted to establish a difference between the effects of fabric anisotropy and effective stress on soil stiffness. A similar approach using a multiaxial triaxial cell equipped with bender/extender elements was adopted by [28] to assess the evolution of elastic anisotropy under axially symmetric stress conditions. Using results backed by experiments, ref. [29] carried out discrete element method simulations and stated that more contact normal tensors preferred to distribute along the horizontal direction. Reference [30] used three different sample preparation methods to investigate the fabric anisotropy of Hostun sand, where air-pluviated and tamped samples exhibited higher stiffness in the horizontal and vertical directions, respectively.

Most of the previous studies have focused on either of the two aspects: either anisotropy of clean sands or sands with varying fines content. In nature, sands are often mixed with fines, and subjected to anisotropic stress states, possibly due to an existing sub-structure or repetitive loading over time. Therefore, studies combining both fines content under anisotropic stress conditions are necessary considering their practical importance. Therefore, in the present work, the influence of fines content on G_{max} under anisotropic stress conditions was investigated in detail. In addition, the application of e^* in Equation (7) in specimens under anisotropic stress was inspected.

2. Experimental Procedure and Sample Preparation

The following sub-sections describe the experimental device and procedure followed by the tested materials and the method of sample preparation.

2.1. The RC Device

The RC and Bender element tests are common methods to determine the small-strain dynamic properties of soils (e.g., shear wave velocity, shear stiffness and damping). To determine the shear modulus and damping, the RC device available at the Ruhr-Universität Bochum was used. The device is capable of investigating the influence of small (shear strain $\gamma < 10^{-5}$) and medium shear strains ($10^{-3} < \gamma < 10^{-5}$). This free-free mode of vibration, i.e., the bottom and top plates are freely movable ([36]), was employed. This specimen is enclosed by a latex membrane of thickness 0.4 mm. The inserted cylindrical soil sample is subjected to harmonic torsional vibrations about the longitudinal axis by two electromagnetic excitation heads. The generated acceleration is measured with the help of two accelerometers, which then results in the linearly distributed torsion γ over the specimen height. This recorded acceleration is displayed on an oscilloscope as a sinusoidal excitation signal, the frequency of which is varied using a function generator until the resonant frequency f_R is determined. The dynamic shear modulus for the specific load amplitude can then be calculated from f_R ([36]):

$$G = \left(\frac{2\pi f_R}{a} \right)^2 \quad (8)$$

$$a \tan(a) - \frac{J^2}{J_0 J_L} \frac{\tan(a)}{a} = \frac{J}{J_0} + \frac{J}{J_L} \quad (9)$$

The polar mass moment of inertia for the bottom and top parts of the device, as well as the sample, are denoted by J_0 , J_L and J respectively. ρ denotes the sample density, while $a = \frac{\omega L}{v_s}$, ω is the rotational frequency, L is the sample height and v_s the shear wave velocity. The schematic figure of the RC device is shown in Figure 3.

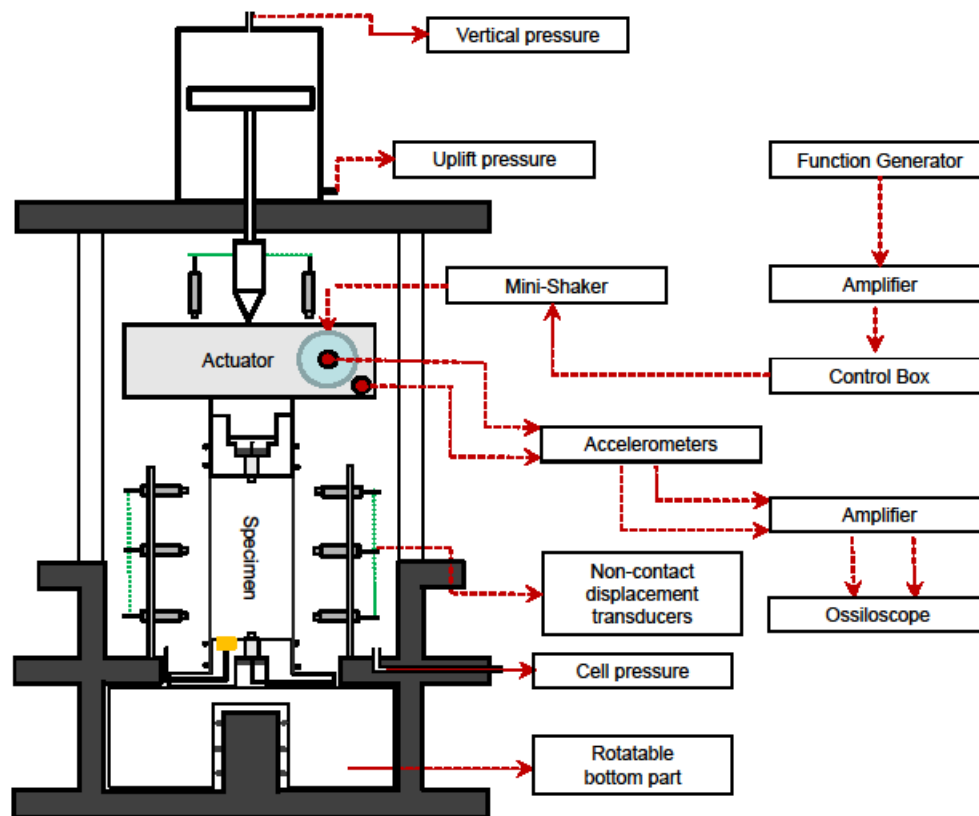


Figure 3. Schematic representation of the RC device used in the present study.

The device was modified for performing tests under anisotropic stress states ([37]). A pneumatic pressure cylinder was mounted on the top of the cell, as shown in Figure 3, for applying vertical pressure on the specimen. The calibration and validation of the device were performed following different methods, further details of which are in [11,37]. At the beginning, the specimen was isotropically loaded with a cell pressure $\sigma'_h = 50$ kPa. From a cell pressure of 200 kPa onwards, the vertical pressure ensures anisotropy in the specimen. The results on isotropically loaded specimens were shown previously in [17]. This paper aimed to describe the results on the same soil mixtures, but under anisotropic loading. The stress path is currently divided into two areas: isotropic condition at $\sigma'_h = 200$ kPa ([11,17]) and anisotropic condition where σ'_h is constant 200 kPa and σ'_v is increased up to 600 kPa (i.e., effective vertical to horizontal stress ratio $\sigma'_v / \sigma'_h = 3$).

2.2. Tested Materials

In the present work, four series of tests were carried out with a mixture of Hostun sand (a quartz sand originally mined in France) and non-plastic quartz (obtained locally) as fines with different proportions by weight—0%, 5%, 10% and 20%. The material mixtures of Hostun sand and the different proportions of fines are shown in Figure 4. The white opaque parts show the quartz powder and the light-colored elements denote sand particles. Hostun sand has been used previously in numerous tests ([37]). Silica is the predominant chemical that constitutes the sand grains ($\text{SiO}_2 > 98\%$). The sand is angular with a grain density of 2.65 g/cm^3 . The mean grain size of Hostun sand and quartz powder (also consisting of SiO_2 as the main component) is 0.375 mm and 0.004 mm, respectively. Figure 5 shows the grain size distribution of the tested materials obtained following [38].

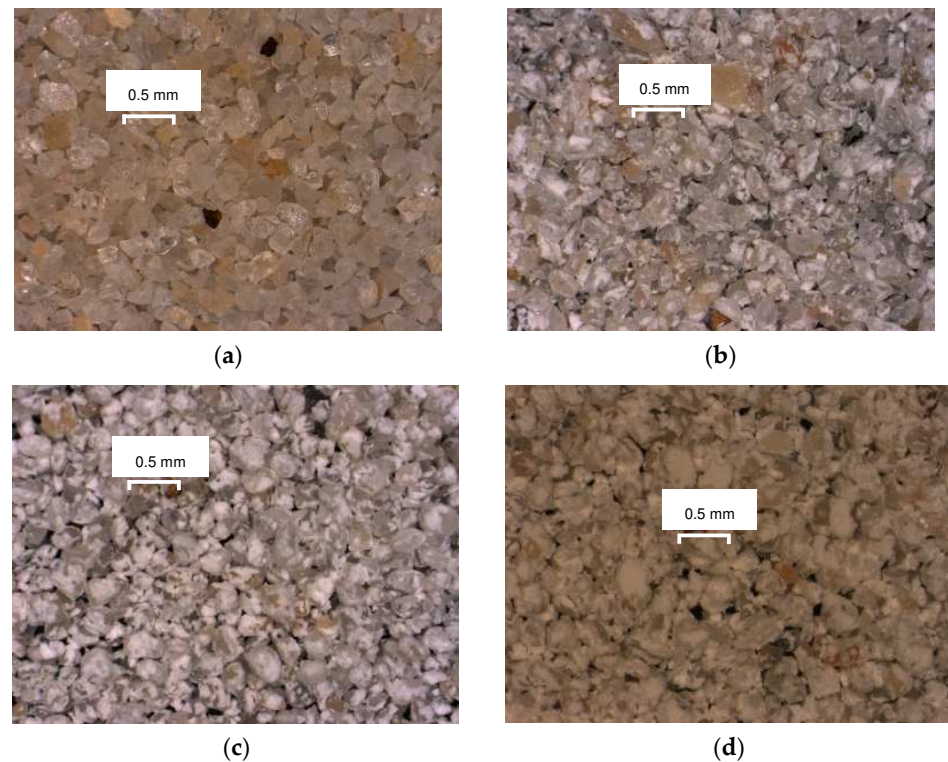


Figure 4. (a) Clean Hostun sand and sand mixed with (b) 5%, (c) 10% and (d) 20% quartz fines used in the present study.

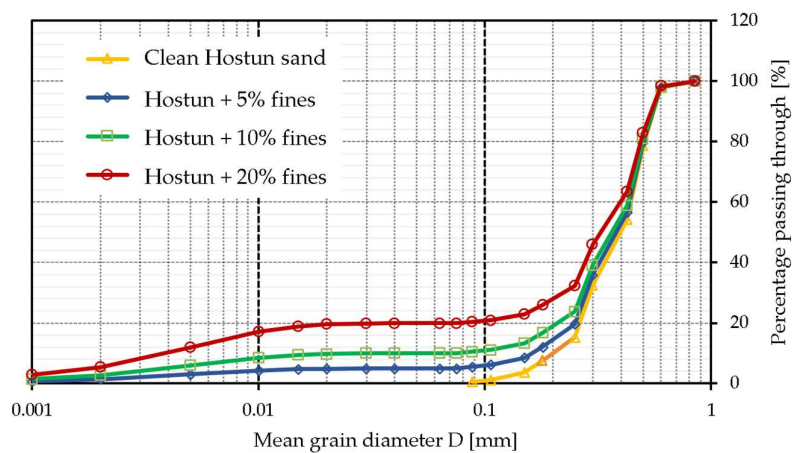


Figure 5. Grain size distribution of the tested materials.

3. Experimental Results

From Figure 6a–d, the influence of the anisotropic stress on the variation in void ratio e over different fines content is shown. The results show that with an increase in the effective anisotropic deviatoric stress σ'_v/σ'_h , the e decreases with increasing fines, whereas the decrease is minimal for the clean sand (Figure 6a). This implies a higher compressibility of the mixtures with higher fines.

Furthermore, Figure 7 shows the relationship between G_{max} , e and σ'_v/σ'_h . It is clear that the G_{max} increases with decreasing e and increasing $\frac{\sigma'_v}{\sigma'_h}$. It is interesting to note the relative magnitudes of the G_{max} for differing fines content—it is higher for the clean Hostun sand (Figure 7a) but reduces with increasing fines content. In addition, the reduction in G_{max} is much larger at higher fines content, although the specimens are prepared at an

initially dense state (see Figure 7d). Practically, the influence of e is diminished at $f_c = 20\%$, while it is largest at $f_c = 0\%$.

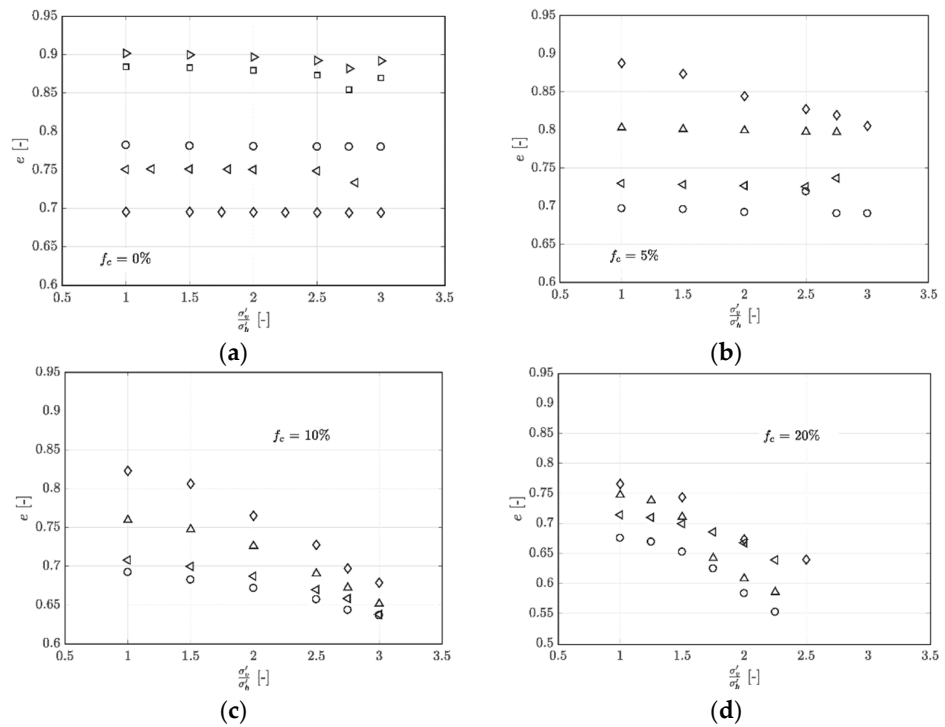


Figure 6. Void ratio e vs. anisotropic stress for (a) clean Hostun sand and sand mixed with (b) 5%, (c) 10% and (d) 20% fines, respectively.

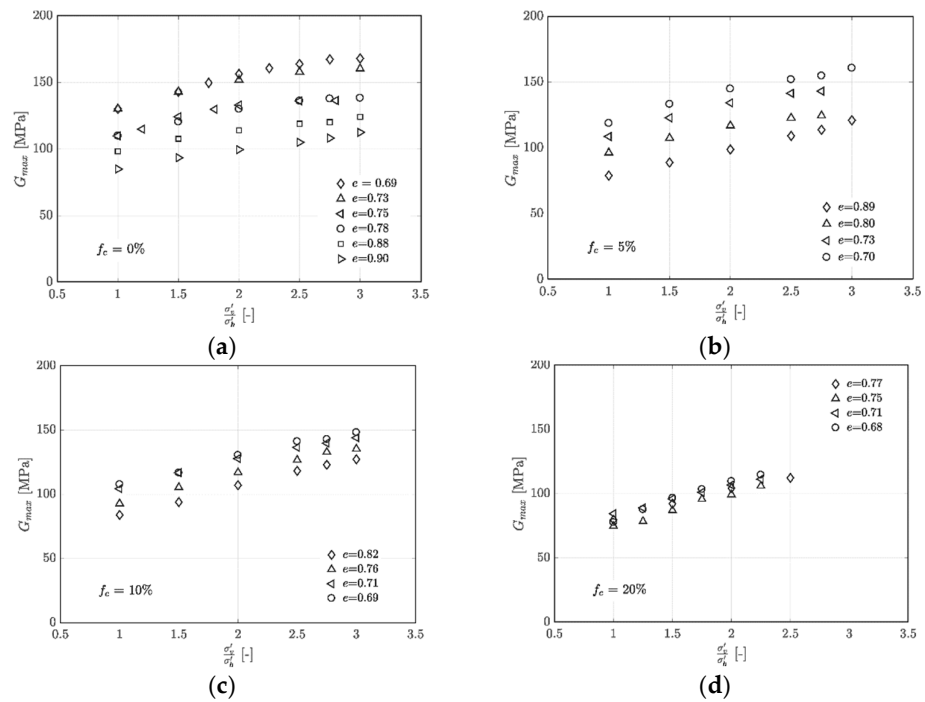


Figure 7. The influence of the anisotropic stress on the G_{max} for (a) clean Hostun sand and sand mixed with (b) 5%, (c) 10% and (d) 20% fines, respectively.

In Figure 8, the variation of the G_{max} with different e and f_c values is shown along with isotropic (Figure 8a) and anisotropic (Figure 8b) states. For all specimens with 0%, 5%,

10% and 20% fines content, G_{max} decreases with the increase in e and increase of vertical stress, σ'_v . In comparison to the isotropic specimen with initial $e = 0.80$ and containing 5% fines, the 20% fines specimen under the same boundary conditions shows a lower G_{max} —for 5% f_c , which is close to 100 MPa, while for the other, it measures around 75 MPa. The same trend can be noted for the anisotropic specimen in Figure 8b, which implies an increase in anisotropic stress load causes an increase in the maximum shear modulus, whereas the increase in f_c causes a reduction in the maximum shear modulus.

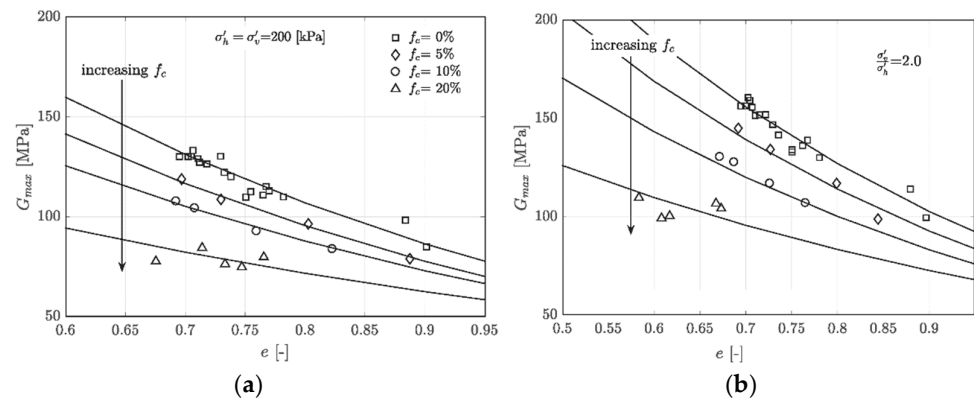


Figure 8. Variation of the G_{max} with different void ratios and fines content under (a) isotropic and (b) anisotropic stress states.

For $\sigma'_v/\sigma'_h = 2$, the G_{max} for clean sand measures approximately 160 MPa at $e = 0.70$ (Figure 8b), while under isotropic conditions (Figure 8a), it measures around 135 MPa. This reinforces the observation that at anisotropic stress conditions, an increase in the e as well as fines content results in a significant decrease in the G_{max} .

4. Analysis of Results

Using the popular models of [1,23], the variation in the G_{max} with e , p' and $\sigma'_v/\sigma'_h = 1$ (isotropic) and 2 (anisotropic) was quantified as shown in Figure 9. In general, a good fit with the experimental data can be seen. Later, the G_{max} was normalized with the void ratio function employing an average value of the fitting parameter c ($= 2.12, 2.15, 2.37$ and 3.25 for 0%, 5%, 10% and 20% fines, respectively). To capture the variation in the anisotropic stress, the G_{max} was initially normalized with the Hardin's void ratio function, considering the average value of the fitting parameter c ($= 2.12, 2.15, 2.37$ and 3.25 for 0%, 5%, 10% and 20% fines, respectively), following which the normalized G_{max} was further plotted against the σ'_v/σ'_h (shown only for the clean sand case in Figure 10a) to obtain the best fit magnitudes of the fitting parameters n_v and n_h . Figure 10b presents a 3D overview of the variation of G_{max} with regards to e , σ'_v and σ'_h (Equation (10) in the case of the clean sand only, shown in Figure 10b below, where the proposed model shows a good fit with the experimental data with $R^2 = 0.95$ (K_0 denotes the ratio σ'_h/σ'_v).

$$\frac{G_{max}}{f(e)} = 0.836 p_a \left(\frac{\sigma'_v}{p_a} \right)^{0.21} \left(\frac{\sigma'_h}{p_a} \right)^{0.23} \quad (10)$$

However, it is not possible to capture in a single curve the influence of varying fines content. Therefore, as suggested by various studies, the global void ratio can also be replaced by the equivalent granular void ratio e^* , which would have the same magnitude as e for clean sand but would depend on the parameter b for fine content below the threshold fines. Based on the suggestion of [20] from their experiments with 10 sands, a value of 30% was deemed suitable for the f_{thr} since it was able to capture many characteristic responses of undrained soil behavior regardless of host sands. The b value was calculated accordingly in order to convert the e to e^* up to a fines content of 20%. The resulting $G_{max} - e^*$ curves for both isotropic and anisotropic stress states are shown in Figure 11 below. The data at

higher e^* and lower G_{max} show relatively greater scatter than at lower e^* and higher G_{max} . Hardin’s relationship also shows a slight deviation to higher e^* and lower G_{max} , which may be attributed to the inherent variability of G_{max} . Figure 12 shows a comparison of the measured and predicted G_{max} with the proposed Equation (10), where a good fit is evident ($R^2 = 0.80$) for different f_c values ranging between 0–20% as well as different degrees of anisotropy achieved by loading in the vertical direction ($1 \leq \sigma'_v/\sigma'_h \leq 3$).

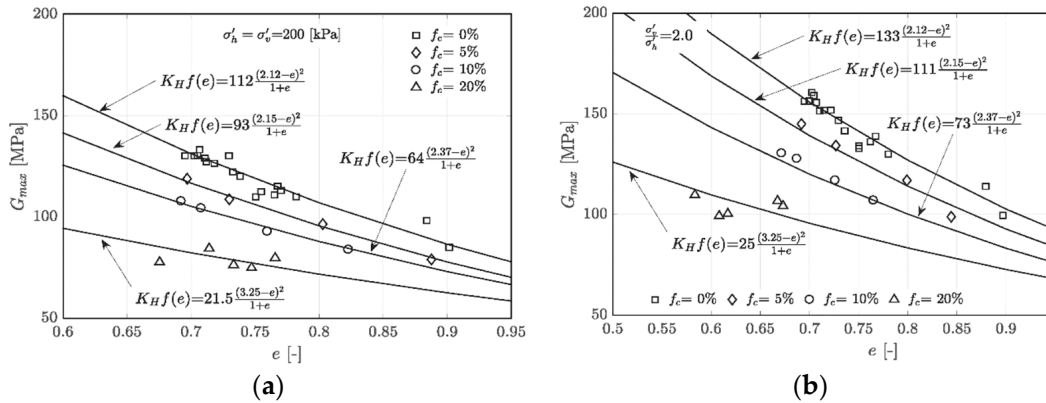


Figure 9. Prediction of the G_{max} with different void ratios and fines content under (a) isotropic and (b) anisotropic stress states. The lines denote the best fits obtained using the Hardin void ratio equation, $K_H f(e)$.

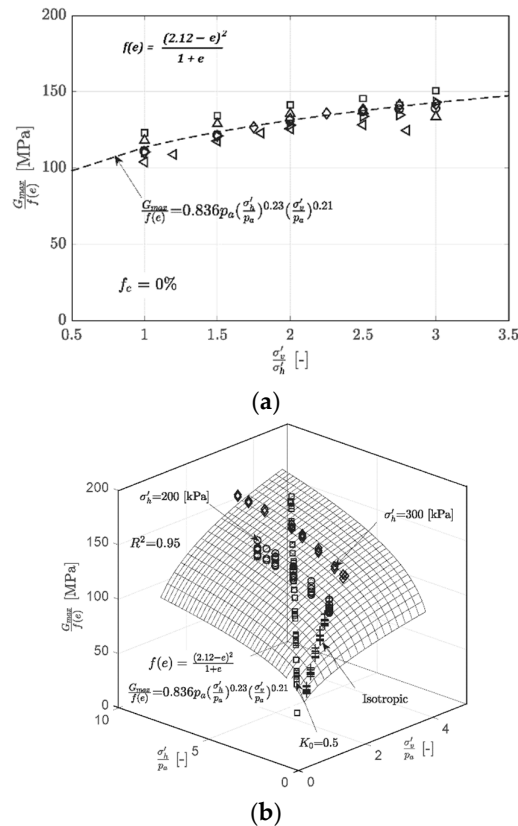


Figure 10. (a) Variation of the normalized G_{max} (using the Hardin void ratio function) with the horizontal and vertical stresses accounting for both isotropic and anisotropic states; (b) 3D representation of the same (also shown in [39]).

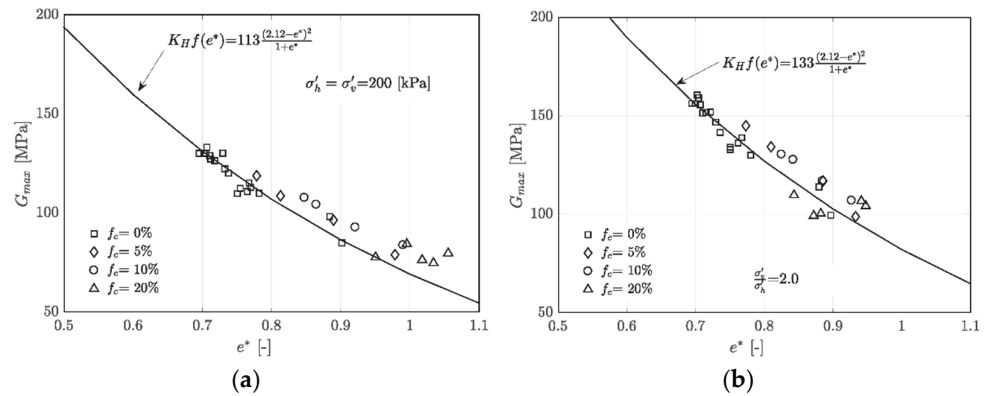


Figure 11. Using e^* instead of e to predict G_{max} under (a) isotropic and (b) anisotropic stress states.

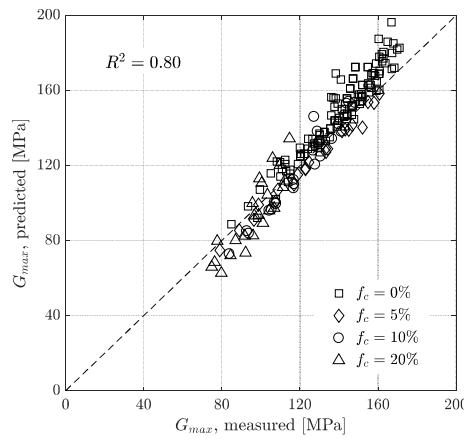


Figure 12. Comparison of the measured and predicted G_{max} values considering different fines content.

5. Discussion

As shown in the previous section, by using e^* instead of e in the Hardin’s model, it was possible to capture the influence of varying fines lower than the threshold value. The biggest advantage afforded by using e^* is that one can avoid the numerous back calculations to determine the fitting parameters for each fines content. In addition, a solid micromechanical interpretation based on certain existing studies employing similar concepts [40–44] asserts a more logical approach, which, presently, is achieved via the b parameter—a micromechanical parameter specially designed to account for the positive or negative effects of f_c or the micromechanical influence of f_c in fine sand mixtures, and can be roughly estimated if the grain size distribution is available.

Micromechanical Interpretation

The stiffness of soil samples depends on microstructural properties, mainly grain-to-grain contacts that dictate the stiffness of the material. According to the theory of Hertz–Mindlin, the tangential or shear stiffness K_T between two grains is a function of the normal stiffness K_N , contact forces f_T and f_N and the elastic properties of the grains ([45,46]), and is mathematically represented as:

$$K_T = C_2 K_N \left[1 - \frac{f_T}{f_N \tan \varphi} \right]^\eta \tag{11}$$

$$K_N = C_1 f_N^n \tag{12}$$

$$\eta = n = \frac{1}{3} \tag{13}$$

n and η are fitting parameters. With the increase in the vertical load f_N , the normal stiffness increases, which results in increments in the friction and, consequently, the tangential stiffness and shear modulus G_{max} between particles. An additional load applied in the vertical direction results in an increase in f_T . However, according to Equation (11), an increase in f_T should result in a decrease in K_T , which explains the slower increase in G_{max} for anisotropic stresses compared to G_{max} for isotropic cases.

Presently, to reinforce our observations, a micro-CT scan was performed on the sample having 10% fines content in Kumamoto University in Japan (Figure 13a). The sample height and diameter for the CT scan was 40 mm and 7 mm, respectively (Figure 13b). Three densities were selected: loose ($\rho = 1.207 \text{ g/cm}^3$, Figure 14a), medium-dense ($\rho = 1.312 \text{ g/cm}^3$, Figure 14b) and dense ($\rho = 1.437 \text{ g/cm}^3$, Figure 14c), details of which are in Table 1. The white particles denote sand grains, while those in gray denote fines, i.e., the quartz powder. From Figure 14a, the fines cover some of the coarse particles merely like a coating. Some of the fine grains arrange themselves between the coarse particles, i.e., these fine grains actively interact with the sand grains. The remaining fine grains distribute themselves in the voids between the coarse grains, i.e., these parts of the fine grains act inertly ([17]). An external load causes friction between the individual grains. For large grains, the friction surface is correspondingly large, making the grain-to-grain contact system relatively stable. Adding more fine grains (Figure 14b,c) reduces the friction area between the individual grains, causing the system to lose stability. Mathematically, this results in a lower contact force K_T and thus results in a lower maximum shear stiffness ([10]).

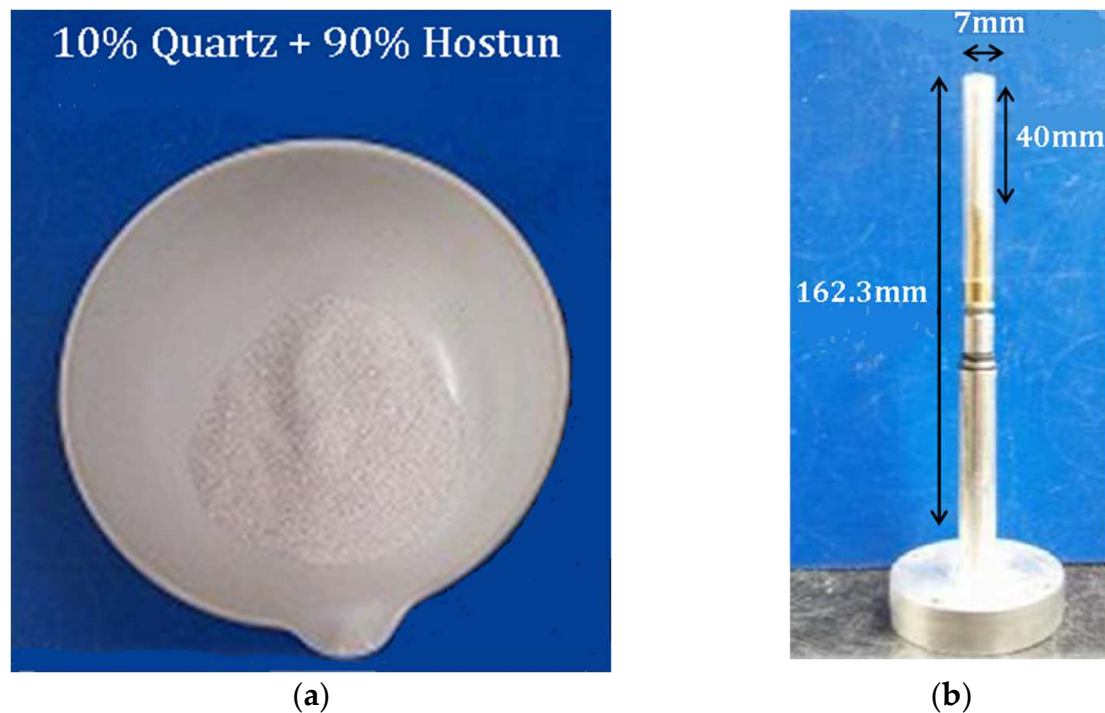


Figure 13. (a) Mixture of 10% quartz and 90% Hostun sand; (b) typical sample for micro-CT analysis.

Table 1. Schedules of the various samples for micro-CT analysis for different densities.

Case	Material	Weight Ratio (%)		Sample Height (mm)	Weight (g)	Dry Density (g/cm^3)
		Quartz	Hostun			
1				37.5		1.207
2	Quartz/Hostun	10	90	34.5	1.742	1.312
3				31.5		1.437

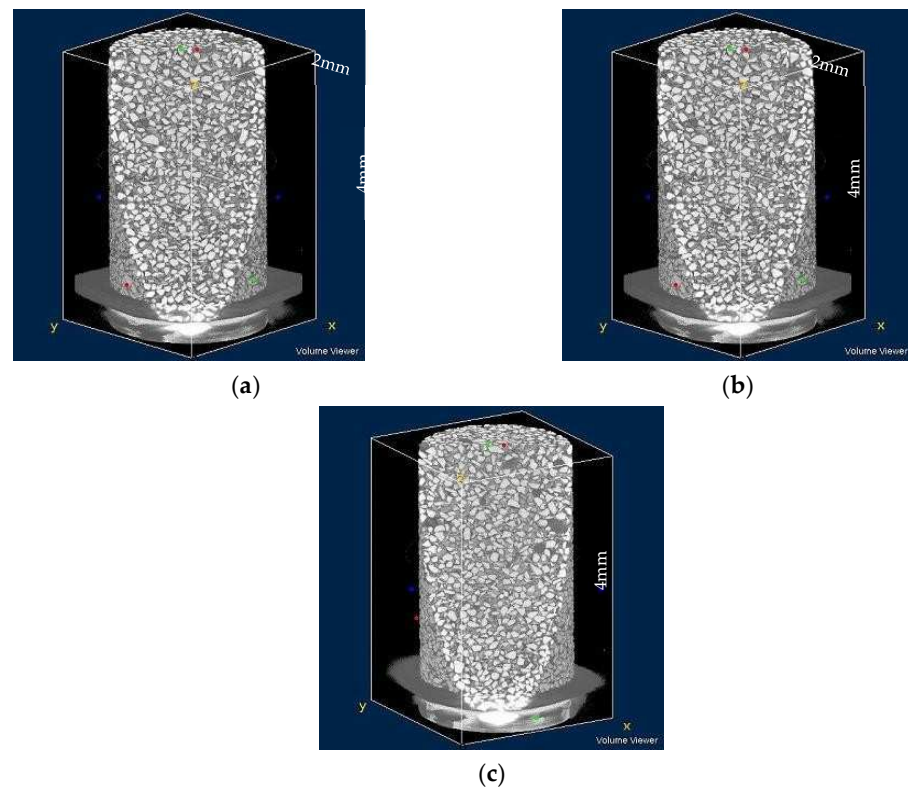


Figure 14. Micro-CT scan images for (a) loose, (b) medium-dense and (c) dense specimens for 10% fines content.

6. Conclusions

The aim of the study was to demonstrate the variation of the maximum shear modulus in binary mixtures of sand–non-plastic fines considering stress anisotropy due to additional vertical loading. As already mentioned, individual studies considering stress anisotropy or mixtures were conducted in previous research, however this work presents one of the first considering both these influences. This paper briefly summarizes the results and interpretation of the tests with respect to the influence of stress anisotropy and fine grain content on the G_{max} . The major findings are summed up below:

- Based on a series of resonant column tests with different initial global void ratios and confining pressures, it was found that G_{max} is lower for increasing fines content as well as higher void ratios. Using a popular empirical model, the variation of G_{max} with void ratio, confining pressure and stress state was captured with a good accuracy.
- Furthermore, to include fines content, the concept of equivalent intergranular void ratio was used where the global void ratio e was replaced by e^* in the various formulations with a higher degree of accuracy, particularly for lower magnitudes of e^* .
- Micro-CT scans of the binary mixtures were additionally made to enable a closer look into the microstructure, e.g., grain-to-grain contacts. From the skeletal structure, the contact forces between the individual grains were evident. In the case of anisotropic stress, a shear force acts in addition to the normal force for isotropically loaded specimens. An increase in fines results in a reduction in the friction between sand grains which leads to lower contact stiffness.

The results of the present work will provide practical knowledge for design engineers to predict the shear modulus in binary mixtures considering the designed overburden vertical stress leading to a stress anisotropy, and therefore, allow them to reliably calculate ground settlements/factor of safety of structures under dynamic loads. Furthermore, advanced constitutive models can also incorporate both these influencing factors in complex multi-variable numerical simulations.

For future work, the influence of stress anisotropy and grain distribution on elastic modulus E , grain shape or size and grain minerals can be investigated. In addition, the influence of other stress paths can be checked. Furthermore, a higher percentage of fines greater than 20% can be investigated. For a more accurate interpretation of the results, various methods, such as the discrete element method (DEM), to determine the number of grain contacts or the force distribution on the grains can be applied.

Author Contributions: Conceptualization, M.G.; methodology, M.G.; validation, M.G.; formal analysis, M.G.; writing—original draft preparation, D.S.; writing—review and editing, M.G. and D.S. All authors have read and agreed to the published version of the manuscript.

Funding: This research received no external funding.

Institutional Review Board Statement: Not applicable.

Data Availability Statement: Not applicable.

Acknowledgments: The authors would like to acknowledge the student Huma Randjoor for assisting in the experiments. Furthermore, the authors would like to dedicate this work in the memory of the late Tom Schanz, who was instrumental with his ideas, and without whose support, the research would not have been successfully accomplished. The authors are further grateful to Kumamoto University, Japan for providing us the micro-CT scans of the materials in 2014.

Conflicts of Interest: The authors declare no conflict of interest.

References

- Hardin, B.O.; Black, W.L. Sand stiffness under various triaxial stresses. *J. Soil Mech. Found. Div.* **1966**, *92*, 27–42. [[CrossRef](#)]
- Drnevich, V.P. *Resonant-Column Testing: Problems and Solutions*; Technical Report; Dynamic Geotechnical Testing: ASTM International, USA, 1978; pp. 384–398.
- Seed, B.; Wong, R.; Idriss, I.; Tokimatsu, K. *Moduli and Damping Factors for Dynamic Analyses of Cohesionless Soils*; Technical Report; National Science Foundation: Alexandria, VA, USA, 1984.
- Jamiolkowski, M.; Lancellotta, R.; Lo Presti, D.C.F. Remarks on the stiffness at small strains of six Italian clays. In Proceedings of the International Symposium, Sapporo, Japan, 12–14 September 1994; pp. 817–836.
- Darendeli, M.B. Development of a New Family of Normalized Modulus Reduction and Material Damping Curves. Ph.D. Thesis, University of Texas at Austin, Austin, TX, USA, 2001.
- Wichtmann, T.; Triantafyllidis, T. On the influence of the grain size distribution curve of quartz sand on the small strain shear modulus. *J. Geotech. Geoenviron. Eng.* **2009**, *135*, 1404–1418. [[CrossRef](#)]
- Thevanayagam, S. Effect of fines and confining stress on undrained shear strength of silty sands. *J. Geotech. Geoenviron. Eng.* **1998**, *124*, 479–491. [[CrossRef](#)]
- Salgado, R.; Bandini, P.; Karim, A. Shear strength and stiffness of silty sand. *J. Geotech. Geoenviron. Eng.* **2000**, *126*, 451–462. [[CrossRef](#)]
- Wichtmann, T.; Navarrete Hernández, M.A.; Triantafyllidis, T. On the influence of a non-cohesive fines content on small strain stiffness, modulus degradation and damping of quartz sand. *Soil Dyn. Earthq. Eng.* **2015**, *69*, 103–114. [[CrossRef](#)]
- Goudarzy, M.; König, D.; Schanz, T. Small strain stiffness of granular materials containing fines. *Soils Found.* **2016**, *56*, 756–764. [[CrossRef](#)]
- Goudarzy, M.; König, D.; Santamarina, J.C.; Schanz, T. Influence of anisotropic stress state on the intermediate strain behaviour of granular materials. *Geotechnique* **2018**, *68*, 221–232. [[CrossRef](#)]
- Iwasaki, T.; Tatsuoka, F. Effects of grain size and grading on dynamic shear moduli of sands. *Soils Found.* **1977**, *17*, 19–35. [[CrossRef](#)]
- Tao, M.; Figueroa, J.; Saada, A. Influence of non-plastic fines content on the liquefaction resistance of soils in terms of the unit energy. In *Cyclic Behavior of Soils and Liquefaction Phenomena*; CRC Press: Boca Raton, FL, USA, 2004.
- Chien, L.K.; Oh, Y.N. Influence of fines content and initial shear stress on dynamic properties of hydraulic reclaimed soil. *Can. Geotech. J.* **2002**, *39*, 242–253. [[CrossRef](#)]
- Carraro, J.A.H.; Prezzi, M.; Salgado, R. Shear strength and stiffness of sands containing plastic or non-plastic fines. *J. Geotech. Geoenviron. Eng.* **2009**, *135*, 1167–1178. [[CrossRef](#)]
- Yang, J.; Liu, X. Shear wave velocity and stiffness of sand: The role of non-plastic fines. *Geotechnique* **2016**, *66*, 500–514. [[CrossRef](#)]
- Goudarzy, M.; Rahman, M.M.; König, D.; Schanz, T. Influence of non-plastic fine particles on maximum shear modulus of granular materials. *Soils Found.* **2016**, *56*, 973–983. [[CrossRef](#)]
- Goudarzy, M.; König, D.; Schanz, T. Small and intermediate strain properties of sands containing fines. *Soil Dyn. Earthq. Eng.* **2018**, *110*, 110–120. [[CrossRef](#)]

19. Rahman, M.M.; Cubrinovski, M.; Lo, S.R. Initial shear modulus of sandy soils and equivalent granular void ratio. *Geomech. Geoengin.* **2012**, *7*, 219–226. [[CrossRef](#)]
20. Rahman, M.M.; Lo, S.C.R.; Gnanendran, C.T. On equivalent granular void ratio and steady state behavior of loose sand with fines. *Can. Geotech. J.* **2008**, *45*, 1439–1455. [[CrossRef](#)]
21. Rahman, M.M.; Lo, S.C.R.; Gnanendran, C.T. Reply to the discussion by Wanatowski and Chu on “On equivalent granular void ratio and steady state behaviour of loose sand with fines”. *Can. Geotech. J.* **2008**, *46*, 483–486. [[CrossRef](#)]
22. Thevanayagam, S.; Shenthan, T.; Mohan, S.; Liang, J. Undrained fragility of clean sands, silty sands, and sandy silts. *J. Geotech. Geoenviron. Eng.* **2002**, *128*, 849–859. [[CrossRef](#)]
23. Zuo, L.; Baudet, B.A. Determination of the transitional fines content of sand-non plastic fines mixtures. *Soils Found.* **2015**, *55*, 213–219. [[CrossRef](#)]
24. Roesler, S. Anisotropic shear modulus due to stress anisotropy. *J. Geotech. Eng. Div.* **1979**, *105*, 871–880. [[CrossRef](#)]
25. Bellotti, R.; Jamiolkowski, M.; Lo Presti, D.C.; O'Neill, D.A. Anisotropy of small strain stiffness in Ticino sand. *Geotechnique* **1996**, *46*, 115–131. [[CrossRef](#)]
26. Zeng, X.; Ni, B. Stress-induced anisotropic G_{max} of sands and its measurement. *J. Geotech. Geoenviron. Eng.* **1999**, *125*, 741–749. [[CrossRef](#)]
27. Fioravante, V. Anisotropy of small strain stiffness of Ticino and Kenya sands from seismic wave propagation measured in triaxial testing. *Soils Found.* **2000**, *40*, 129–142. [[CrossRef](#)]
28. Sadek, T.; Lings, M.; Dihoru, L.; Wood, D.M. Wave transmission in Hostun sand: Multi-axial experiments. *Riv. Ital. Geotech.* **2007**, *2*, 69–84.
29. Wang, Y.; Mok, C. Mechanisms of small strain shear modulus anisotropy in soils. *J. Geotech. Geoenviron. Eng.* **2008**, *134*, 1516–1530. [[CrossRef](#)]
30. Ezaoui, A.; Di Benedetto, H. Experimental measurements of the global anisotropic elastic behaviour of dry Hostun sand during triaxial tests, and effect of sample preparation. *Geotechnique* **2009**, *59*, 621–635. [[CrossRef](#)]
31. Yanagisawa, E. Influence of void ratio and stress condition on the dynamic shear modulus of granular media. *Adv. Mech. Flow Granul. Mater.* **1983**, *2*, 947–960.
32. Yu, P.; Richart, F. Stress ratio effects on shear modulus of dry sands. *J. Geotech. Eng.* **1984**, *110*, 331–345. [[CrossRef](#)]
33. Ishibashi, I.; Chen, Y.; Chen, M.T. Anisotropic behavior of Ottawa sand in comparison with glass spheres. *Soils Found.* **1991**, *31*, 145–155. [[CrossRef](#)]
34. Santamarina, C.; Cascante, G. Stress anisotropy and wave propagation: A micromechanical view. *Can. Geotech. J.* **1996**, *33*, 770–782. [[CrossRef](#)]
35. Payan, M.; Khoshghalb, A.; Senetakis, K.; Khalili, N. Small-strain stiffness of sand subjected to stress anisotropy. *Soil Dyn. Earthq. Eng.* **2016**, *88*, 143–151. [[CrossRef](#)]
36. Wichtmann, T.; Sonntag, T.; Triantafyllidis, T. Über das Erinnerungsvermögen von Sand unter zyklischer Belastung. *Bautechnik* **2001**, *78*, 852–865. [[CrossRef](#)]
37. Goudarzy, M. Micro and Macro Mechanical Assessment of Small and Intermediate Strain Properties of Granular Material. Ph.D. Thesis, Ruhr-Universität Bochum, Bochum, Germany, 2015.
38. *DIN 18126:1996-11*; Baugrund, Untersuchung von Bodenproben—Bestimmung der Dichte Nichtbindiger Böden bei Lockerster und Dichtester Lagerung. Beuth: Berlin, Germany, 1996. (In German)
39. Goudarzy, M.; König, D.; Schanz, T. Interpretation of small and intermediate strain characteristics of Hostun sand for various stress states. *Soils Found.* **2018**, *58*, 1526–1537. [[CrossRef](#)]
40. Bohaienko, V.; Bulavatsky, V. Fractional-Fractal Modeling of Filtration-Consolidation Processes in Saline Saturated Soils. *Fractal Fract.* **2020**, *4*, 59. [[CrossRef](#)]
41. He, S.; Ding, Z.; Hu, H.; Gao, M. Effect of Grain Size on Microscopic Pore Structure and Fractal Characteristics of Carbonate-Based Sand and Silicate-Based Sand. *Fractal Fract.* **2021**, *5*, 152. [[CrossRef](#)]
42. Fu, X.; Ding, H.; Sheng, Q.; Zhang, Z.; Yin, D.; Chen, F. Fractal Analysis of Particle Distribution and Scale Effect in a Soil–Rock Mixture. *Fractal Fract.* **2022**, *6*, 120. [[CrossRef](#)]
43. Xu, J.; Shen, Y.; Sun, Y. Cyclic Mobilisation of Soil–Structure Interface in the Framework of Fractional Plasticity. *Fractal Fract.* **2022**, *6*, 76. [[CrossRef](#)]
44. Adeli, E.; Rosic, B.V.; Matthies, H.G.; Reinstädler, S.; Dinkler, D. Bayesian Parameter determination of a CT-Test described by a Viscoplastic-Damage model considering the Model Error. *Metals* **2020**, *10*, 1141. [[CrossRef](#)]
45. Yimsiri, S.; Soga, K. Application of micromechanics model to study anisotropy of soils at small strains. *Soils Found.* **2002**, *42*, 15–26. [[CrossRef](#)]
46. Johnson, K.L. *Contact Mechanics*; Cambridge University: Cambridge, UK, 1985.